



## Adhesion Control for Freight Train Based on Improved Sliding Mode Extremum Seeking Algorithm and Barrier Lyapunov Function

Xiang Cheng<sup>1\*</sup>, Jing He<sup>2</sup>, Changfan Zhang<sup>2</sup>, Gang Huang<sup>2</sup>, Yishan Huang<sup>3</sup>

<sup>1</sup> College of Intelligent Control of Railway Transportation, Hunan Railway Professional Technology College, Zhuzhou 412000, Hunan, China

<sup>2</sup> College of Electrical and Information Engineering, Hunan University of Technology, Zhuzhou 412000, Hunan, China

<sup>3</sup> CRRC Electric Vehicle Co., Ltd., Zhuzhou 412000, Hunan, China

Corresponding Author Email: [chengxiang@stu.hut.edu.cn](mailto:chengxiang@stu.hut.edu.cn)

<https://doi.org/10.18280/jesa.550205>

### ABSTRACT

**Received:** 4 March 2022

**Accepted:** 19 April 2022

#### Keywords:

*adhesion control, extremum seeking, particle swarm algorithm, barrier Lyapunov function, parameter estimation*

Adhesion control system is an essential component for a freight train, which aims to optimize its performance of traction, the design of the adhesion control system remains a significant challenge. One of the main challenges is the optimal creep-speed is difficult to acquire in real-time, the other one is the parameters of resistance were not available in advance. Meanwhile, adhesion is a nonlinear dynamical process. In this paper, an improved sliding mode extremum seeking virtual sensors is proposed for the issue of acquiring the optimal creep-speed in real-time; a particle swarm algorithm (PSO)-based estimation method is proposed for the issue of uncertain resistance parameters; and finally, an adhesion controller is designed based on the barrier Lyapunov concept.

## 1. INTRODUCTION

Adhesion control systems play an important role in improving the traction performance of freight trains [1]. Numerous studies have shown that the adhesion coefficient between wheels and rails is related to the creep speed, and it is practical to improve the adhesion performance of a railroad vehicle by the creep speed control [2]. Creep speed is generally defined as the difference between the wheel speed and the vehicle speed, when the creep speed is optimally matched with the current rail surface conditions, the vehicle can obtain the maximum traction [3]. Under the premise that the creep speed is known, some scholars have carried out a series of adhesion control studies. However, the maximum creep speed is varied, when the train travels on different track surfaces [4], the artificially given creep speed does not match the actual working conditions of railroad vehicles [5]. The extremum seeking algorithm is usually used to acquire the optimal creep speed, the commonly used extremum seeking methods are sliding mode extremum seeking (SMEs) and single parameter perturbation extremum seeking (SPEs), among which SMEs has been introduced into the adhesion control field due to its simple parameter structure and high robustness.

For example, Zhao et al. [6] used a state observer to estimate the current rail adhesion coefficient and then introduced SMEs to acquire the optimal creep speed, but severe oscillation appeared in the output of the observer, due to the obvious nonlinear phenomenon of adhesion. Zhao et al. [6] designed an adhesion control strategy combining a full-dimensional state observer and SMEs. However, the oscillation of the search results is obvious because the parameters of the SMEs cannot be dynamically adjusted. He and Yuan [7] considered the oscillation problem of the adhesion coefficient observer. A SMEs was first performed for the optimal creep speed, and

then a fractional order controller was designed to reduce the oscillation of the output torque. STMC uses lower-order differentiation to eliminate oscillation to some extent, but oscillation in SMEs is inherently present. Usually, the adhesion control based on the extremum seeking algorithm is to construct an observer to estimate the real-time adhesion coefficient first, and then use the optimal creep speed obtained from the extremum seeking as the tracking index, and use the output of the traction motor as the control quantity, but the high-frequency oscillation generated during the observation of the adhesion coefficient and the extremum seek stage will eventually lead to a large oscillation of the control torque, which will have a relatively negative impact on the safety and comfort of driving.

To improve the oscillation problem in SMEs, a series of researches have been carried out. For example, B Viola et al. [8] proposed an FO-SMESC algorithm using the fractional-order method, which achieved oscillation weakening but the algorithm itself was too complicated. Lamzouri et al. [9] proposed a SMES based on particle swarm algorithm optimization, but greatly increased the complexity of the algorithm, while not considering the effect of uncertain parameters. The SMEs algorithm was originally designed to achieve system control with simple parameters and high robustness, existing improvement methods generally introduce an algorithm of higher complexity for minor defects in the original SMEs. In this paper, we dissect the principle of SMEs, and an improved method based on threshold switching is proposed, which not only does not increase the complexity of the original algorithm but also can eliminate the steady-state oscillation. The PSO algorithm is introduced to estimate the parameters of train running resistance, providing a new optimal design method for freight train adhesion control.

This paper is organized as follows: according to the

dynamics model of a freight train is introduced in Section 2. A control strategy based on improved SMES is designed to ensure the optimal creep speed can be locked (without steady-state oscillation) and effective adhesion control, which is discussed in Section 3. Comparative simulations and analyses are illustrated in Section 4. Finally, this paper's conclusion is given in Section 5.

## 2. DYNAMICS MODEL OF FREIGHT TRAIN

### 2.1 Freight train model with unknown parameters

The equations of motion of the freight train and the wheel dynamic model are described as follows:

$$M\dot{v}_t = F_a - F_z \quad (1)$$

$$J\dot{\omega}_m = T_m - T_L \quad (2)$$

$$v_d = \omega r \quad (3)$$

In the above equation,  $M$  is the mass of the car body,  $\omega_m$  is the rotation speed of traction motor,  $v_t$  is the train body forward speed,  $v_d$  is the linear speed of the wheels,  $\omega$  is the angular speed of the wheels;  $r$  is the radius of the wheels,  $T_m$  is the driving torque of the traction motor,  $T_L$  is the load torque of the freight train;  $F_a$  is the adhesive force of the vehicle,  $F_z$  is the driving resistance of the vehicle, the driving resistance can be expressed as follows [10]:

$$F_z = a_1 + a_2 v_t + a_3 v_t^2 \quad (4)$$

In the above equation, is the number greater than zero, different driving environment parameters take different values and cannot be directly given [11], this paper will be driving resistance parameters as the amount to be identified, the use of particle swarm algorithm for its estimation.

The expression of adhesion force and load torque can be shown as follows:

$$F_a = \mu W g \quad (5)$$

$$T_L = \frac{F_a r}{R_g} \quad (6)$$

The adhesion force is not only related to the adhesion coefficient  $\mu$ , but also highly related to the axial weight  $W$ , in which  $g$  is the acceleration of gravity,  $R_g$  is the gear ratio; in addition, the adhesion coefficient also has a highly non-linear relationship with the creep speed  $v_s$ , and the expression of the relationship between the two is generally as follows [12]:

$$\mu = c(e^{-av_s} - e^{-bv_s}) \quad (7)$$

$$v_s = v_d - v_t \quad (8)$$

where,  $a$ ,  $b$ ,  $c$  are track surface parameters, different track surface conditions, and their parameters are shown in Table 1.

### 2.2 Description of the adhesion constraint

The adhesion process of freight trains has high nonlinear characteristics, taking the dry rail surface as an example (see Figure 1), the changing law of the adhesion characteristics curve of the rest of the rail surface is similar. In the adhesion zone, the adhesion coefficient increases gradually with the increase of creep speed; in the slipping zone, the adhesion coefficient decreases rapidly with the increase of creep speed. The constraint problem of adhesion control is to constrain the adhesion point as much as possible to a small neighborhood of the peak of the adhesion characteristic curve. In other words, by controlling the creep speed within a small neighborhood of the optimal creep speed, wheel spin or slip can be avoided.

**Table 1.** Different track surface adhesion parameters

Type	Parameters			Optimal adhesion coefficient
	$a$	$b$	$c$	
dry	0.54	1.0	1.2	0.286
wet	0.54	0.72	0.206	0.206

The union of (1), (2), (4), and (5) yields:

$$\dot{v}_s = \frac{1}{M} [F_a - (a_1 + a_2 v_t + a_3 v_t^2)] - \frac{r}{JR_g} T_m + \frac{r^2}{JR_g^2} F_a \quad (9)$$

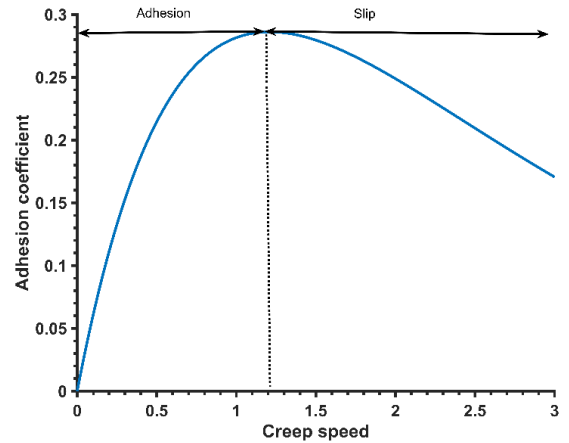


**Figure 1.** Dry rail surface adhesion characteristics curve

The adhesion control constraint in this paper can be expressed as:

$$v_s \leq v_{sopt} \quad (10)$$

In the above equation  $v_{sopt}$  is the optimal creep speed of the driving track surface. If the control law is designed to satisfy the Eq. (10), the train can be guaranteed to travel under better adhesion conditions and thus maximize tractive force.

## 3. CONTROL STRATEGY BASED ON IMPROVED SMES

The adhesion control framework proposed in this paper is to first design an observer to estimate the adhesion coefficient, and then design the PSO to estimate the parameters of the resistance force. Then the improved SMES strategy is designed, in which, when the SMES algorithm converges to

the target value, the output of the observer is switched into an extremum seeking algorithm (ESA) without steady oscillations to lock the optimal creep speed; finally, the controller is designed to achieve the vehicle adhesion control through the optimal creep speed tracking.

### 3.1 Adhesion coefficient observer

In Eq. (2), the motor rotation speed  $\omega_m$  is measurable and the load torque  $T_L$  is unknown, taking the rotation speed as the state variable, a full-dimensional state observer of the load torque is designed as follows [13]:

$$\begin{cases} \dot{\hat{x}} = A\hat{x} + Bu + L(y - \hat{y}) \\ \hat{y} = C\hat{x} \end{cases} \quad (11)$$

in which,  $A = \begin{bmatrix} 0 & -\frac{1}{J_m} \\ 0 & 0 \end{bmatrix}$ ,  $B = \begin{bmatrix} \frac{1}{J_m} \\ 0 \end{bmatrix}$ ,  $C = [1 \ 0]$ ,  $L = [L_1 \ L_2]$ ,  $u = T_m$ ,  $x = [\omega_m \ T_L]^T$ ,  $y = \omega_m$ ,  $L$  is the observer gain matrix,  $L_1$  and  $L_2$  are gain parameters of the observer to be designed the value of  $L$  (shown in Table 2).  $\hat{T}_L$  is the observed value of load torque ( $T_L$ ),  $\hat{x}$  and  $\hat{y}$  are observed values of  $x$  and  $y$ ,  $\hat{\mu}$  is the observed value of adhesion coefficient, the observation of  $T_L$  can be obtained using the pole placement method.

$$\hat{T}_L = \int L_2(\omega_m - \hat{\omega}_m) dt \quad (12)$$

Once we have the observed value of  $T_L$ , the observed value of the adhesion coefficient  $\mu$  can be obtained by Eq. (5).

$$\hat{\mu} = \frac{R_g}{rWg} \hat{T}_L \quad (13)$$

### 3.2 Resistance parameter identification with PSO

There are two forces in the dynamic equations of freight trains that cannot be measured directly, one is the adhesion between the wheels and rails [14] and the other is the driving resistance [15]. From Eq. (5), it can be seen that the adhesion force is linearly related to the adhesion coefficient under certain axle weight, and the estimated value of the adhesion force can be deduced from the observation of the adhesion coefficient. While there is no way to directly measure the driving resistance, Eq. (4) is an empirical formula for the resistance under statistical significance, but the resistance parameters in it cannot be obtained in advance, and the PSO algorithm [16] is introduced in this subsection to estimate the resistance parameters.

Selecting the train speed and wheel angular velocity as state variables, rewrite Eqns. (1)-(4) as follows:

$$\begin{cases} M\dot{v}_t = F_a - a_1 - a_2v_t - a_3v_t^2 \\ J\dot{\omega} = T_m - T_L \end{cases} \quad (14)$$

Let  $x_1 = v_t$ ,  $x_2 = \omega$ ,  $u = T_m$ , then

$$\begin{cases} \dot{x}_1 = F_a / M - (1/M) \cdot a_1 - (1/M)a_2x_1 - (1/M)a_3x_1^2 \\ \dot{x}_2 = x_3 \\ \dot{x}_3 = (1/J)u - (1/J)T_L \end{cases} \quad (15)$$

Rewrite Eq. (15) as follows:

$$\eta Y = \tau \quad (16)$$

$$\eta = \begin{bmatrix} \frac{1}{M}a_2 & \frac{1}{M}a_3 & 1 & \frac{1}{M}a_1 & \frac{1}{M}F_a & 0 \\ 0 & 0 & 0 & T_L & 0 & J \end{bmatrix} \quad (17)$$

$$Y = [x_1 \ x_1^2 \ \dot{x}_1 \ 1 \ -1 \ \dot{x}_3]^T \quad (18)$$

$$\tau = \begin{bmatrix} 0 \\ u \end{bmatrix} \quad (19)$$

The parameters to be identified in the travel resistance are  $a_1$ ,  $a_2$ ,  $a_3$ , according to the principle of least squares, we get:

$$\eta = \tau(Y^T Y)^{-1} Y^T \quad (20)$$

The index of the discrimination error is designed as:

$$J = \sum_{i=1}^N \frac{1}{2} (\tau_i - \hat{\tau}_i)^2 \quad (21)$$

$N$  is the dimensionality of the input signal,  $\tau_i$  is the input of the  $i$ th sample of the model.

In addition, dynamic weighting method  $w(i) = ((w_{\max} - w_{\min}) / \sqrt{2\pi}) \exp[-\frac{i}{G}(w_{\max} - w_{\min})^2]$  and unbalanced learning factor ( $c_1=0.4, c_2=0.1$ ) strategy are used in this paper to improve the local optimum of the algorithm,  $w(i)$  is the weight of the  $i$ th iteration,  $G$  is the maximum number of iterations,  $w_{\min} = 0.1, w_{\max} = 0.8$ .

### 3.3 Improved SMEs algorithm

One of the difficulties in the adhesion control of freight trains is how to lock the best creep speed of the current track surface [17], and it is known from Section 1.2 that the adhesion characteristic curve has obvious polar characteristics, with the real-time adhesion coefficient of the vehicle as input and the best creep speed of the current track surface as the output, the commonly used creep speed SMEs structure is shown in Figure 2.

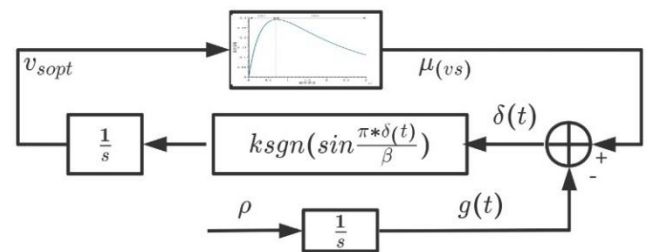


Figure 2. Creep speed SMEs structure

The mathematical representation of the SMEs structure represented in Figure 2 can be shown as follows:

$$\begin{cases} \delta(t) = \mu(v_s) - g(t) \\ \dot{v}_{sopt} = k \operatorname{sgn}(\sin(\frac{\pi \delta(t)}{\beta})) \end{cases} \quad (22)$$

In Figure 2,  $g(t)$  is the auxiliary function of the extreme value search, and its first-order derivative is  $\rho$ . The sliding mode function is  $\delta(t)=\mu-g(t)$ .  $k$  is the gain of the SMEs. From the principle of SMEs [18] and trigonometric formula, we have:

$$\sin\left(\frac{\pi^*\delta(t)}{\beta}\right) = 2\sin(\pi\delta(t)/2\beta)\cos(\pi\delta(t)/2\beta) \quad (23)$$

Define the replacement function as follows:

$$s_1 = 2\sin(\pi\mu_0/2\beta) \quad (24)$$

$$s_2 = \cos(\pi\mu_0/2\beta) \quad (25)$$

The corresponding sliding modes are:

$$\frac{\delta(t)}{\beta} = \begin{cases} 2n, r_1 = 0 \\ 2n+1, r_2 = 0 \end{cases}, n=0, \pm 1, \pm 2... \quad (26)$$

From Eq. (24-25), we have:

$$\begin{cases} \dot{s}_1 = \frac{\pi}{2\beta} \cos(\pi\delta(t)/2\beta) \frac{d}{dt} \delta(t) \\ s_1 \dot{s}_1 = \frac{\pi}{4\beta} \sin\left(\frac{\pi\delta(t)}{\beta}\right) \left[ \frac{d\mu}{dv_s} k \operatorname{sgn}\left(\sin\frac{\pi\delta(t)}{\beta}\right) - \rho \right] \end{cases} \quad (27)$$

$$\begin{cases} \dot{s}_2 = \frac{\pi}{2\beta} \sin(\pi\delta(t)/2\beta) \frac{d}{dt} \delta(t) \\ s_2 \dot{s}_2 = -\frac{\pi}{4\beta} \sin\left(\frac{\pi\delta(t)}{\beta}\right) \left[ \frac{d\mu}{dv_s} k \operatorname{sgn}\left(\sin\frac{\pi\delta(t)}{\beta}\right) - \rho \right] \end{cases} \quad (28)$$

Obviously, when  $2n < \delta(0) < 2n+1$ ,  $s_1 \dot{s}_1 \leq 0$  if  $\frac{d\mu}{dv_s} < \frac{\rho}{k}$ . At this time,  $s_1 \rightarrow 0$ ,  $\delta(t) \rightarrow 2n\beta$ ; when  $(2n+1)\beta < \delta(0) < (2n+2)\beta$ ,  $s_1 \dot{s}_1 \leq 0$  if  $\frac{d\mu}{dv_s} < -\frac{\rho}{k}$ , at this time,  $s_1 \rightarrow 0$ ,  $\delta(t) \rightarrow (2n+2)\beta$ ; when  $2n\beta < \delta(0) < (2n+1)\beta$ ,  $s_2 \dot{s}_2 \leq 0$  if  $\frac{d\mu}{dv_s} > \frac{\rho}{k}$ , at this time  $s_2 \rightarrow 0$ ,  $\delta(t) \rightarrow (2n+1)\beta$ ; when  $(2n+1)\beta < \delta(0) < (2n+2)\beta$ ,  $s_2 \dot{s}_2 < 0$  if  $\frac{d\mu}{dv_s} > -\frac{\rho}{k}$ ,  $\delta(t) \rightarrow (2n+1)\beta$ . From the above analysis, it is clear that as long as  $\left| \frac{d\mu}{dv_s} \right| > \frac{\rho}{k}$  is satisfied, SMEs will converge in finite time, and oscillations of amplitude  $(-k, k)$  are generated in the steady-state phase. The design idea of this subsection is to switch the input to ESA without steady-state oscillation. However, since the extremum cannot be known in advance, it is not appropriate to use  $\left| \frac{d\mu}{dv_s} \right| < \frac{\rho}{k}$  directly as the switching threshold. The new switching thresholds are designed as follows.

As shown in Figure 2, at the initial moment:

$$\delta_0 = \mu_0 \quad (29)$$

$f_0$  refers to the initial value, in this case  $g_0 = 0$ , so the above equation can be rewritten as:

$$\frac{\delta_0}{\beta} = \frac{\mu_0}{\beta} \quad (30)$$

The derivative expression of the estimated creep-slip velocity is:

$$\dot{v}_s = k \operatorname{sgn}(\sin(\pi\mu_0/\beta)) \quad (31)$$

According to the trigonometric formula, we have:

$$\sin(\pi\mu_0/\beta) = 2\sin(\pi\mu_0/2\beta)\cos(\pi\mu_0/2\beta) \quad (32)$$

Define the replacement function as follows:

$$\gamma_1 = 2\sin(\pi\mu_0/2\beta) \quad (33)$$

$$\gamma_2 = \cos(\pi\mu_0/2\beta) \quad (34)$$

The corresponding sliding modes are:

$$\frac{\mu_0}{\beta} = \begin{cases} 2n, r_1 = 0 \\ 2n+1, r_2 = 0 \end{cases} \quad (35)$$

When the initial value  $\mu_0$  converges to the sliding mode plane  $[\mu_0/\beta]$  or  $[\mu_0/\beta] \pm \beta$ , the seeking output is close to the maximum value of  $\mu$ . Considering the possible misjudgment caused by oscillation, this paper selects  $[\mu_0/\beta] - 3\beta$  as the threshold. The improved SMEs framework is shown in Figure 3.

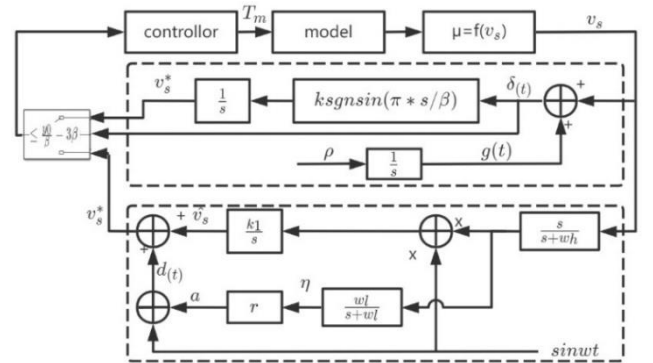


Figure 3. Improved SMEs framework

In the lower part of Figure 3, the dashed box shows the ESA without oscillation.  $\sin \omega t$  is the excitation signal,  $k_1$  is the integral gain, and  $\omega_h$ ,  $\omega_l$  is the cutoff corner frequency of the high-pass/low-pass filter, respectively.  $r$  is the constant gain. The threshold switching is performed when the SMEs is judged to be close to the extreme value, which is equivalent to an ESA with the initial value near the extreme value point.

### 3.3.1 Stability analysis

For the convenience of expression, note  $\theta(v_s) = d\mu/dv_s$ , and define the optimal creeping slip velocity as  $v_s^*$ . From the principle of SMEs, it follows that for any given parameter  $\rho/k > 0$ , there exists a positive constant  $\beta$  such that the steady-state value of  $\theta(v_s)$  satisfies  $|\theta(v_s)| \leq \rho/k$ . The following setting is given.

$$v_{s1} = \Theta^{-1}(\rho/k), v_{s2} = -\Theta^{-1}(\rho/k), v_s^* = \Theta^{-1}(0) \quad (36)$$

$$e_{v_s^*} = \max \left\{ |v_{s1} - v_s^*|, |v_{s2} - v_s^*| \right\} \quad (37)$$

$e_{v_s^*}$  is the extremum-seeking error of the SMEs under the condition  $|\theta(v_s)| \leq \rho/k$ . From Eq. (30), it can be seen that for a given positive constant  $e$ , there is a corresponding  $\rho/k$  such that  $e_{v_s^*} \leq e$  holds, where  $e$  is the error of the ESA without oscillation. Then, the  $v_s$  after threshold switching lies in the convergence domain of the ESA without oscillation.

### 3.4 Controller design

Adhesion control is an atypical output-constrained problem, specifically, the control process aims to restrict the wheel-track adhesion state within the optimal area domain. In this paper, after achieving the optimal creep speed, we design the adhesion controller based on the barrier Lyapunov function with the locked  $v_s^*$  as the tracking target to achieve the active control of optimal creep tracking. Define the tracking error of creep speed as  $e_s$  and its derivative expression as follows:

$$\dot{e}_s = f(x) - g(x)T_m - \dot{v}_s^* \quad (38)$$

$$f(x) = \left(\frac{1}{M} + \frac{r^2}{JR_g^2}\right)F_a - \frac{1}{M}F_z \quad (39)$$

$$g(x) = \frac{r}{JR_g} \quad (40)$$

In the above equation,  $F_a$  can be calculated indirectly by the adhesion coefficient observer, the resistance parameters have been designed PSO algorithm for identification, and  $v_s^*$  are locked by the extreme value search module. For the convergence of the tracking error, the barrier Lyapunov function [19] is designed as follows.

$$V = \frac{1}{4}(1 - \text{sgn}(e_s)) \log \frac{k_a^2}{k_a^2 - e_s^2} + \frac{1}{4}(1 + \text{sgn}(e_s)) \log \frac{k_s^2}{k_s^2 - e_s^2} \quad (41)$$

The definition domain of the above equation is divided into two parts:  $D_1 = \{e \in R: -k_a < e_s < k_a\}$ ,  $D_2 = \{e \in R: -k_s < e_s < k_s\}$ , where  $D_1$  is used to delineate the overall obstacle boundary so that the value of  $k_a$  is greater than the maximum creep speed, Construct the constraint using  $D_2$  when  $v_s$  exceeds  $v_s^*$ , its schematic diagram is shown in Figure 4.

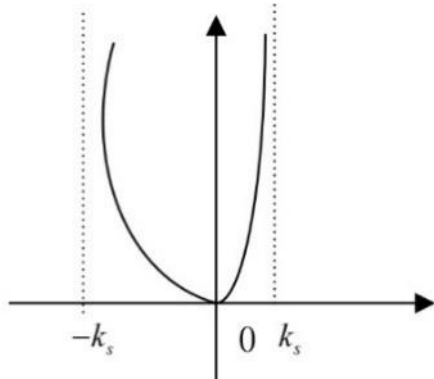


Figure 4. Schematic diagram of the barrier Lyapunov

For the tracking problem of the optimal creep speed, the output torque of the traction motor is chosen as the control quantity and the following control law is designed.

$$u = \frac{1}{g(x)} (-f(x) + \dot{v}_s^* - k_1 e_s (1 - \text{sgn}(e_s))(k_a^2 - e_s^2) - (1 + \text{sgn}(e_s))k_2 e_s (k_s^2 - e_s^2)) \quad (42)$$

For the proposed control law, stability proofs are carried out as follows:

Case1: when  $e_s < 0$ ,  $\text{sgn}(e_s) = -1$ , the barrier Lyapunov becomes the following form:

$$V_1 = \frac{1}{4}(1 - \text{sgn}(e_s)) \log \frac{k_a^2}{k_a^2 - e_s^2} \quad (43)$$

The control law at this point becomes:

$$u_1 = \frac{1}{g(x)} (-f(x) + \dot{v}_s^* - (1 - \text{sgn}(e_s))k_1 e_s (k_a^2 - e_s^2)) \quad (44)$$

Taking Eq. (38) into Eq. (37) gives

$$\begin{aligned} \dot{V}_1 &= \frac{e_s \dot{e}_s}{k_a^2 - e_s^2} = \frac{e_s}{k_a^2 - e_s^2} (f(x) + g(x)u_1 - \dot{v}_s^*) \\ &= -2k_1 e_s^2 < 0 \end{aligned} \quad (45)$$

Case2: when  $e_s > 0$ ,  $\text{sgn}(e_s) = 1$ , the barrier Lyapunov becomes the following form:

$$V_2 = \frac{1}{4}(1 + \text{sgn}(e_s)) \log \frac{k_s^2}{k_s^2 - e_s^2} \quad (46)$$

The control law at this point becomes:

$$u_2 = \frac{1}{g(x)} (-f(x) + \dot{v}_s^* - (1 + \text{sgn}(e_s))k_2 e_s (k_s^2 - e_s^2)) \quad (47)$$

Taking Eq. (41) into Eq. (40), we get:

$$\begin{aligned} \dot{V}_2 &= \frac{e \dot{e}}{k_s^2 - e^2} = \frac{e}{k_s^2 - e^2} (f(x) - g(x)u_2 - \dot{v}_s^*) \\ &= -2k_2 e^2 < 0 \end{aligned} \quad (48)$$

Case3: when  $e=0$ , from Eq. (39) and Eq. (42) it can be deduced that  $\dot{V}_1 = \dot{V}_2 = 0$ . Stability proof finished.

## 4. SIMULATION AND ANALYSIS

Table 2. Simulation model parameters

parameters	Value
quality of freight train	6000t
single axle weight	30t
wheel diameter	0.625m
gear ratio	6.294
gain parameters for observer	$L_1 = L_2 = -40$
resistance	$F_z = 0.5 + 0.04v + 0.0026v^2$

To verify the effectiveness of the adhesion control strategy of the freight train proposed in this paper, computer simulation is used to verify. The model parameters are shown in Table 2.

#### 4.1 Simulation of resistance parameter identification

When the closed-loop system was constructed, the adhesion force can be deduced using the adhesion coefficient estimated by the observer, but the travel resistance parameters cannot be measured directly. In this paper, a parameter estimation algorithm based on PSO is designed, the specific algorithm parameters are shown in Table 3, its simulation results are shown in Figure 5, and its convergence process is shown in Figure 6.

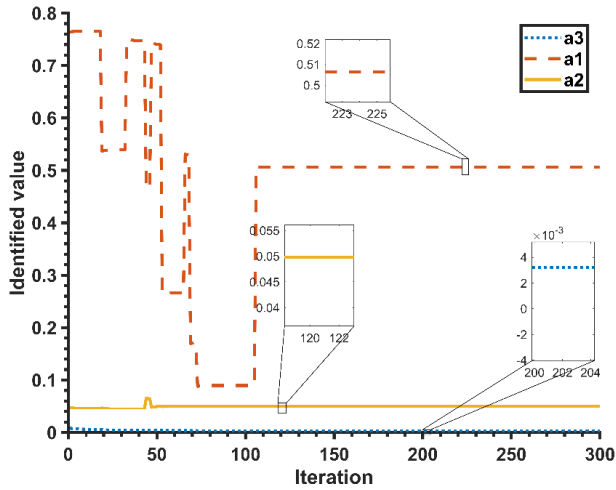


Figure 5. PSO parameter identification results

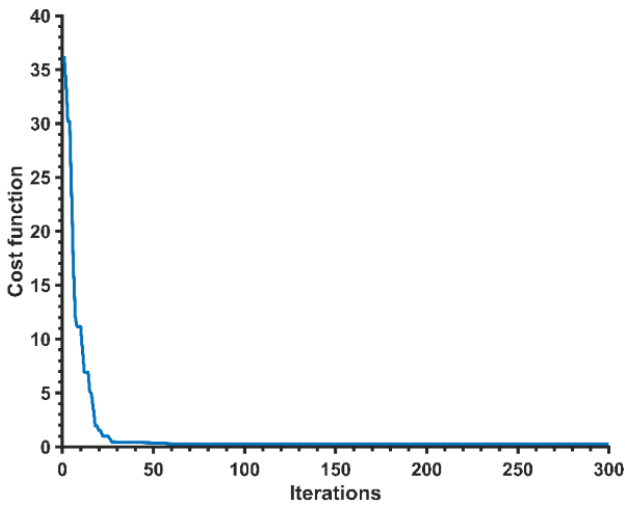


Figure 6. PSO convergence process

Table 3. PSO algorithm parameters

parameters	value
The velocity of particle motion	$[-0.001, 0.001]$
Population size	60
Learning Factors	$c_1 = 0.4, c_2 = 0.1$
Inertia weights	$[0.1, 0.8]$
Maximum number of iterations	300

To verify the parameter identification capability of the PSO algorithm, the actual values of the drag parameters set in this

section are shown in Table 2. From Figure 5, it can be seen that the final convergence values of the algorithm are about  $a_1 = 0.505, a_2 = 0.05, a_3 = 0.003$ . The PSO algorithm can identify the freight train running resistance parameters properly.

#### 4.2 Comparison of extremum seeking

A sudden change of rail surface simulation is designed to verify the optimal creep speed search of the rail surface. 1-10s the vehicle travels on a dry rail surface; at the 10<sup>th</sup> second, the rail surface jumps from dry to wet; and then at the 15<sup>th</sup> second, the vehicle travels back to a dry rail surface. The parameters of the improved extremum search algorithm designed in this paper are as follows.

$k = 1, \beta = 0.1, \rho = 1, \omega_l = 0.7, \omega_h = 0.9$ , constant gain is 1. The improved SMEs simulation adhesion coefficient seeking results are shown in Figure 7, which shows that the final locked maximum adhesion coefficient of dry rail surface is 0.2855, which is very close to the actual optimal value of 0.286; the locked maximum adhesion coefficient of wet rail surface is 0.206, which is the same as the actual optimal value. Under the same conditions, the results of the conventional SMEs simulation are shown in Figure 8, the results of ESA simulation are shown in Figure 9.

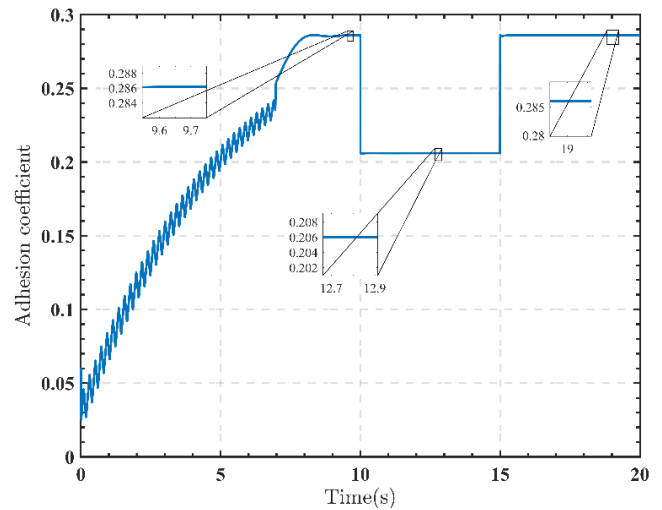


Figure 7. Improved SMEs result

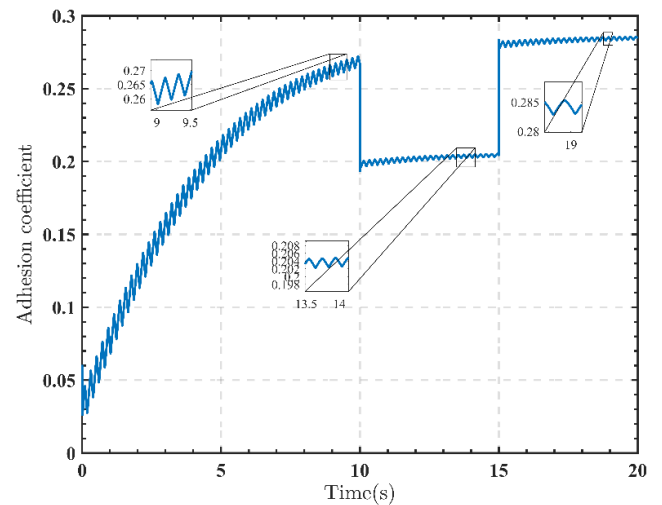


Figure 8. SMEs result

From the comparison of Figures 7, 8 and 9, it can be seen that the improved SMEs has smoothly locked the optimal value at the 8<sup>th</sup> moment, and the traditional SMEs did not fully converge to the extreme value in the dry section until the moment of rail surface switching, the search curve is still an incremental trend. It can be seen from the local enlarged figure that it finally converges to the region where the adhesion coefficient is 0.28 and produces oscillation; while the conventional SMEs algorithm in the wet phase converges to the extreme value point though. However, there are still oscillations with a smaller amplitude and higher frequency, and such high-frequency oscillations bring certain hindrances to the driving safety and smoothness. As Figure 9 shows that the ESA did not converge to the extreme point in the dry section, then the rail surface is switched, the performance at the switching moments is not as smooth as SMEs.

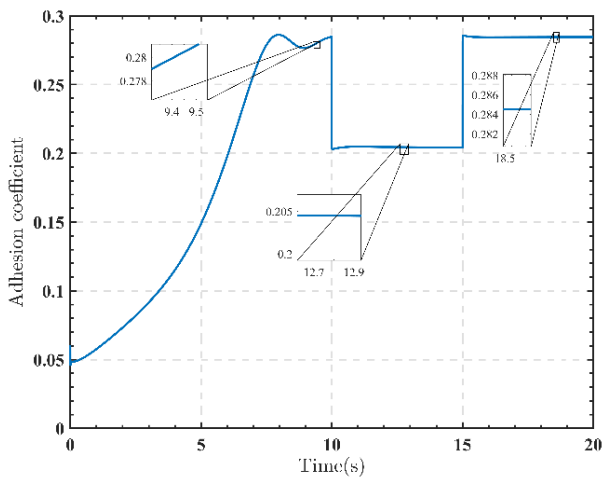


Figure 9. ESA result

The control torque based on the traditional SMEs is shown in Figure 10, the control torque based on the improved SMEs is shown in Figure 11, and the control torque based on the ESA is shown in Figure 12. In the control law,  $k_a = k_b + v_{sopt}$ ,  $k_b = 0.02$ ,  $k_1 = k_2 = 1200$ .

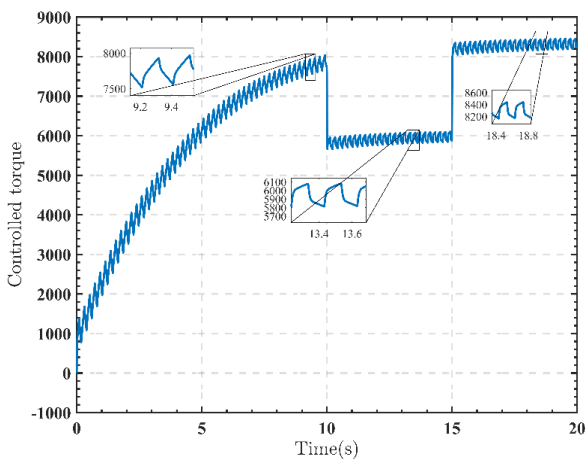


Figure 10. SMEs control torque

The comparison between Figure 10 and Figure 11 shows that the adhesion control torque applying the improved SMEs remains smooth after the algorithm converges, while the adhesion control based on the conventional SMEs converges more slowly and is accompanied by high-frequency

oscillations throughout. Therefore, the improved SMEs-based adhesion control not only has a shorter convergence time but also has better dynamic performance and improves the smoothness of the control torque output.

From the comparison between Figure 11 and Figure 12, it can be seen that the control torque value based on SMEs can reach more than 8300 in the dry stage, while the ESA-based one can only reach about 8250, with similar results in the rest of the stages. This is because the SMEs-based method utilizes the SME algorithm in the initial stage, and as can be seen in the figure, the SMEs-based image is a convex function, while the ESA is a concave function in the initial stage, precisely because of the introduction of the ESA. Therefore, after the threshold switch, the initial value of the coefficient of adhesion based on the SMEs is closer to the true extreme value, and thus the optimal creep-slip speed searched is closer to the actual available maximum value, and thus the output torque of the traction motor can be more fully utilized.

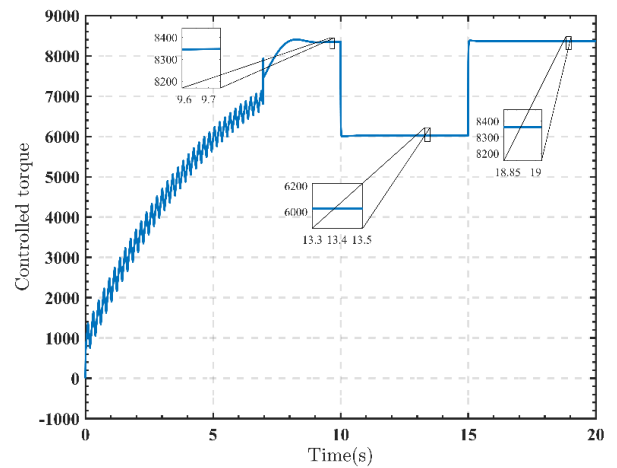


Figure 11. Improved SMEs control torque

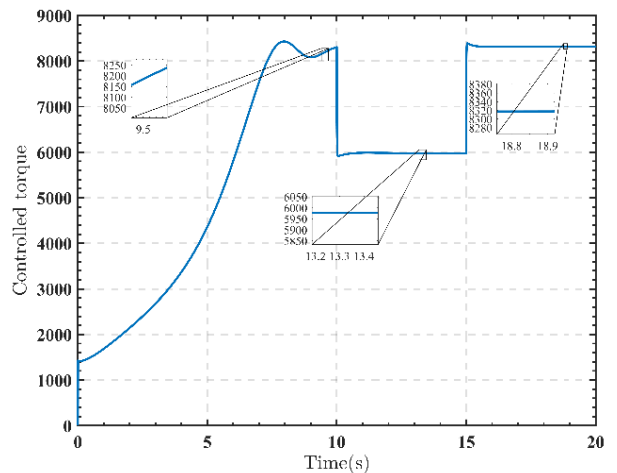


Figure 12. ESA control torque

## 5. CONCLUSION

To address the problem that the real-time optimal adhesion point is difficult to obtain stably and quickly and the travel resistance parameters cannot be measured, this paper proposes a new optimal creep speed seek strategy of improved SMEs combined with PSO algorithm, and finally, the adhesion control law is proposed using the barrier Lyapunov function.

Through the simulation and experimental comparison, the following conclusions are drawn.

(1) The parameter identification model based on PSO is estimated for the unknown parameters in the driving resistance, which effectively ensures the accuracy of parameter identification.

(2) Accurate locking of real-time optimal creep speed using improved SMEs, improves the convergence speed of optimal creep slip seek, and also improves the control accuracy and torque smoothness of traction motor output torque, due to no steady-state oscillations.

(3) The proposed adhesion control law based on the barrier Lyapunov not only guarantees the smooth control of a single rail surface but also maintains the high-precision tracking control of the optimal creep speed under the transient conditions of adhesion, which improves the robustness and dynamic performance of the adhesion control system.

## ACKNOWLEDGMENT

This work is supported by the National Science Foundation of China (Grant numbers: 62173137), and the Scientific Research Project of Hunan Provincial Department of Education (Grant numbers: 21C1295).

## REFERENCES

[1] Huang, D., Yang, W., Huang, T., Qin, N., Tan, Y. (2021). Iterative learning operation control of high-speed trains with adhesion dynamics. *IEEE Transactions on Control Systems Technology*, 99: 1-11. <https://doi.org/10.1109/TCST.2021.3049958>

[2] Chen, B., Huang, Z., Zhang, R., Jiang, F., Liu, W., Li, H., Wang, J., Peng, J. (2020). Adaptive slip ratio estimation for active braking control of high-speed trains. *ISA Transactions*, 112: 302-314. <https://doi.org/10.1016/j.isatra.2020.11.027>

[3] Moaveni, B., Fathabadi, F.R., Molavi, A. (2020). Supervisory predictive control for wheel slip prevention and tracking of desired speed profile in electric trains. *ISA Transactions*, 101: 102-115. <https://doi.org/10.1016/j.isatra.2020.01.011>

[4] Shu, X., Zeng, Y., Wilson, N., Thompson, R., Tajaddini, A. (2019). Wheel/rail contact creep curve measurement and low speed wheel climb derailment investigation. In the IAVSD International Symposium on Dynamics of Vehicles on Roads and Tracks, pp. 660-668. [https://doi.org/10.1007/978-3-030-38077-9\\_77](https://doi.org/10.1007/978-3-030-38077-9_77)

[5] Moaveni, B., Rashidi Fathabadi, F., Molavi, A. (2022). Fuzzy control system design for wheel slip prevention and tracking of desired speed profile in electric trains. *Asian Journal of Control*, 24(1): 388-400. <https://doi.org/10.1002/asjc.2472>

[6] Zhao, K., Li, P., Zhang, C., He, J., Li, X., Liu, J. (2019). Optimal utilization of adhesion force for heavy-haul electric locomotive based on extremum seeking with sliding mode and asymmetric barrier Lyapunov function. *Journal of Advanced Transportation*, 6270515. <https://doi.org/10.1155/2019/6270515>

[7] He, R., Yuan, L. (2020). An improved nonlinear predictive control strategy enhanced by fractional order extremum seeking control of the antilock braking system

of a vehicle. *IEEE Access*, 8: 168576-168588. <https://doi.org/10.1109/ACCESS.2020.3023717>

[8] B Viola, J., Hollenbeck, D., Rodriguez, C., Chen, Y. (2021). Fractional-Order stochastic extremum seeking control with dithering noise for plasma impedance matching. In 2021 IEEE Conference on Control Technology and Applications (CCTA), pp. 247-252. <https://doi.org/10.1109/CCTA48906.2021.9658616>

[9] Lamzouri, F.E., Boufounas, E.M., Brahmi, A., Amrani, A.E. (2020). Optimized TSMC control based MPPT for PV system under variable atmospheric conditions using PSO algorithm. *Procedia Computer Science*, 170: 887-892. <https://doi.org/10.1016/j.procs.2020.03.116>

[10] Wang, F., Ren, L., Ding, J. (2010). *Electric Locomotive Traction Calculation*. Southwest Jiaotong University Press.

[11] Teslenko, D.S., Belyakov, V.V., Makarov, V.S., Dralkin, S.S., Martynov, D.A., Zaitsev, K.I., Zakharkina, K.P. (2021). Methodology for determining the value of resistance to movement of a vehicle as a tool for research and optimization of the shape of the elements of a wheeled vehicle immersed in snow. *Procedia Computer Science*, 186: 138-145. <https://doi.org/10.1016/j.procs.2021.04.132>

[12] Kabzinski, J. (2015). Adaptive, compensating control of wheel slip in railway vehicles. *Bulletin of the Polish Academy of Sciences Technical Sciences*, 63(4): 955-963. <https://doi.org/10.1515/bpasts-2015-0108>

[13] Boutat, D., Zheng, G. (2021). Observability and observer for dynamical systems. In: *Observer Design for Nonlinear Dynamical Systems*. Lecture Notes in Control and Information Sciences, 487. [https://doi.org/10.1007/978-3-030-73742-9\\_1](https://doi.org/10.1007/978-3-030-73742-9_1)

[14] Pichlík, P., Zděnek, J. (2017). Comparison of locomotive adhesion force estimation methods for a wheel slip control purpose. In 2017 9th International Conference on Electronics, Computers and Artificial Intelligence (ECAI), pp. 1-4. <https://doi.org/10.1109/ECAI.2017.8166502>

[15] Altmannshofer, S., Endisch, C. (2016). Robust vehicle mass and driving resistance estimation. In 2016 American Control Conference (ACC), pp. 6869-6874. <https://doi.org/10.1109/ACC.2016.7526754>

[16] Dsnmrao, Kumar, N. (2018). An enhanced reactive power dispatch with finest location of dg using PSO algorithm. *Modelling, Measurement and Control A*, 91(3): 139-144. [https://doi.org/10.18280/mmc\\_a.910306](https://doi.org/10.18280/mmc_a.910306)

[17] Wang, Z., Jia, Y. (2018). A terminal sliding mode algorithm for train velocity tracking considering wheel-rail adhesion. In 2018 Chinese Automation Congress (CAC), pp. 3065-3069. <https://doi.org/10.1109/CAC.2018.8623720>

[18] Abbadi, A., Hamidia, F., Chiba, Y., Tlemcani, A. (2021). Maximum power point tracking method using sliding mode extremum-seeking algorithm for residential wind turbine. In *Advances in Green Energies and Materials Technology*, 401-408. [https://doi.org/10.1007/978-981-16-0378-5\\_52](https://doi.org/10.1007/978-981-16-0378-5_52)

[19] Jiang, Y., Liu, Z., Chen, Z. (2022). Error-constrained coordinated tracking control for high-order multiagent systems based on barrier Lyapunov function. *International Journal of Control, Automation and Systems*, 20: 1238-1249. <https://doi.org/10.1007/s12555-021-0144-7>